All-optical microwave oscillator assisted by parity-time-symmetry breaking

Xiang Zhu,[1] Yali Huang,[1] Hongxia He,[2] Tong He,[1] and Xianbin Yu[3,*]
[1]*Zhejiang Lab, Hangzhou 311121, China*
[2]*School of Communication Engineering, Hangzhou Dianzi University, Hangzhou 310018, China*
[3]*College of Information Science and Electronic Engineering, Zhejiang University, Hangzhou 310027, China*

(Received 23 February 2024; accepted 31 July 2024; published 15 August 2024)

Parity-time ($\mathcal{PT}$) symmetry provides a new technique for the manipulation of oscillation modes in the field of microwave photonics. In this paper, we conceive and experimentally demonstrate a simple $\mathcal{PT}$-symmetric all-optical microwave oscillator (AOMO) based on a single polarimetric loop, overcoming the challenges of manipulating gain and loss and mutual coupling ratio and perfect control of the geometry in the dual-loop configurations. We also uncover the analytics of the $\mathcal{PT}$-symmetry condition in an AOMO with a detailed nonquantum description. By controlling the polarization rotation angle of the $\mathcal{PT}$-symmetric structure, two mutually coupled loops with balanced gain and loss are easily conceived, enabling the proposed AOMO to operate in the single mode. The optical-optical feedback modulation and oscillatory frequency selection are implemented using a semiconductor optical amplifier (SOA) and the stimulated Brillouin scattering (SBS) effect, respectively. Benefiting from the SOA's cross-gain modulation, the SBS-based frequency selection, and the $\mathcal{PT}$-symmetric breaking, dual-wavelength optical signals can be achieved with wideband tunability, very low beating phase noise, and high stability. In the experiment, we successfully generated an oscillating signal tuning from 3 to 30 GHz, and the measured phase noise reached −103.2 dBc/Hz at 10 GHz and −90.69 dBc/Hz at 30 GHz at 10-kHz offset frequency.

DOI: 10.1103/PhysRevA.110.023514

I. INTRODUCTION

An optoelectronic oscillator (OEO) is an important type of microwave photonic oscillator (MPO), which can be used to generate high-quality microwave signals with ultralow phase noise and tunable frequency. In a traditional OEO, an electro-optical modulator and a photodetector with square-law detection are typically used to conduct electrical-to-optical and optical-to-electrical conversions, respectively [1]. To implement stable single-mode oscillation and overcome mode hopping, OEOs based on processes such as dual-loop Vernier effect [2], intermediate frequency (IF) filtering [3], and injection locking have been proposed [4,5]. Usually, the two oscillation loops in a dual-loop OEO feature different lengths, consequently leading to the stability issue as the asymmetric structure is severely affected by the change of operation environment. The IF filtering and injection-locking techniques can improve the OEO stability. However, both require a microwave source with near-carrier low-phase noise to produce an injected electrical signal, making the system bulky and expensive.

Since the first reported implementation of a parity-time ($\mathcal{PT}$) optical coupled system by Rüter *et al.* through the inclusion of index guiding and gain-loss region in 2010 [6], $\mathcal{PT}$ symmetry has been proven to be a powerful technique in cavity-mode selection in recent years [7–9]. By managing the gain, loss, and coupling ratio between the cross-coupled cavities described by the non-Hermitian $\mathcal{PT}$-symmetric Hamiltonians, the $\mathcal{PT}$ symmetry can be broken for stable single-mode oscillation in a cavity laser. The successful fabrication of the $\mathcal{PT}$-symmetric cavity lasers leads the way to create an MPO. Several studies on the applications of $\mathcal{PT}$ symmetry in implementing an OEO have recently been reported [10,11]. By employing a dual-loop with equal lengths and balanced gain and loss, low-phase noise microwave signals of 9.876 GHz in a 9.166 km loop and 4.0703 GHz in a 3.216 km loop were generated. To improve the frequency tunability performance of the $\mathcal{PT}$-symmetric OEOs, a microdisk resonator and the stimulated Brillouin scattering (SBS) effect in a dual loop have also been developed [12,13]. These advances have indicated the $\mathcal{PT}$-symmetric OEOs as a promising solution for effectively suppressing the competing modes and ensuring a stable oscillation. However, realizing the two physically separated macro loops in the $\mathcal{PT}$-symmetric OEOs critically relies on the perfect control of the geometry, gain, loss, and the mutual coupling ratio, complicating the overall system.

Alternatively, a single spatial resonator is recently introduced to greatly improve the stability and simplify the engineering implementation of the $\mathcal{PT}$-symmetric OEOs based on wavelength-division multiplexing (WDM) or polarization-division multiplexing (PDM) techniques [14,15]. The WDM $\mathcal{PT}$-symmetric OEO realizes the equivalent spatially symmetric geometry using two laser sources with different wavelengths in the wavelength space. The PDM uses a z-cut $LiNbO_3$ phase modulator to create two spatial oscillation loops in the polarization space equivalently. It is noted that

*Contact author: xyu@zju.edu.cn

the optical-electrical-optical conversion in these hybrid OEO loops degrades the oscillation efficiency, making it very challenging to generate highly pure frequencies at high frequencies, i.e., in the millimeter-wave and terahertz regions [16]. All-optical microwave oscillators (AOMOs) can potentially avoid such a conversion and generate dual-wavelength optical signals on demand [17,18]. However, only dual-loop structures have been developed, suffering complex implementation and stability issues. To achieve $\mathcal{PT}$ symmetry in the AOMO with a single ring, it should be noted that different from the single spatial resonator based on the WDM technique which uses multiwavelength lasers to achieve $\mathcal{PT}$ symmetry, only one laser signal would be modulated by the feedback due to the gain competition in an AOMO with SOA as the modulator. In addition, the single spatial resonator based on the PDM technique with the z-cut $LiNbO_3$ phase modulator in the oscillation loop cannot be used in the AOMO.

In this paper, we propose and experimentally demonstrate a $\mathcal{PT}$-symmetric AOMO using a single loop. We also uncover the analytics of the $\mathcal{PT}$-symmetry condition in an AOMO with a detailed nonquantum description. For a stable oscillation, the cross-gain modulation (XGM) effect in a semiconductor optical amplifier (SOA) implements optical-optical modulation [19], the SBS effect determines the oscillation frequency, and a single loop with $\mathcal{PT}$ oscillation keeps the system oscillating with a single mode. By adjusting the wavelength spacing between the in-loop laser and the pump laser of SBS, a dual-wavelength optical signal with tunable frequency spacing of 3–30 GHz is generated. This work completes the implementation of $\mathcal{PT}$ symmetry in an AOMO by operating all-fiber polarization control with simple in-line devices, which has the potential to facilitate the practical application and fast integration of the $\mathcal{PT}$-symmetry technique.

II. THE NONQUANTUM DESCRIPTION

Theoretically, a $\mathcal{PT}$-symmetric OEO is usually analyzed by non-Hermitian $\mathcal{PT}$-symmetric Hamiltonians. The coupling equations of the eigenmodes in two cross-coupled loops are given by

$$i\frac{d}{dt}\begin{pmatrix} a_n \\ b_n \end{pmatrix} = \begin{pmatrix} \omega_{a_n} + i\gamma_{a_n} & -\kappa \\ -\kappa & \omega_{b_n} + i\gamma_{b_n} \end{pmatrix}\begin{pmatrix} a_n \\ b_n \end{pmatrix}, \tag{1}$$

where a_n and ω_{a_n} and b_n and ω_{b_n} respectively represent the amplitudes and the angular frequencies of the nth mode in the two loops, κ is the coupling ratio between the two loops, and γ_{a_n} and γ_{b_n} are the gain and loss coefficients in each loop. The eigenfrequencies ω_n^t of the system can then be derived from Eq. (1):

$$\omega_n^t = \frac{\omega_{a_n} + \omega_{b_n}}{2} + i\frac{\gamma_{a_n} + \gamma_{b_n}}{2} \pm \sqrt{\kappa^2 - \left(\frac{\gamma_{a_n} - \gamma_{b_n}}{2} - i\frac{\omega_{a_n} - \omega_{b_n}}{2}\right)^2}. \tag{2}$$

Under the $\mathcal{PT}$-symmetric conditions, there exist $\omega_{a_n} = \omega_{b_n} = \omega_n$ and $\gamma_{b_n} = -\gamma_{a_n} = \gamma_n$. Equation (2) can be therefore simplified as

$$\omega_n^t = \omega_n \pm \sqrt{\kappa^2 - \gamma_n^2}. \tag{3}$$

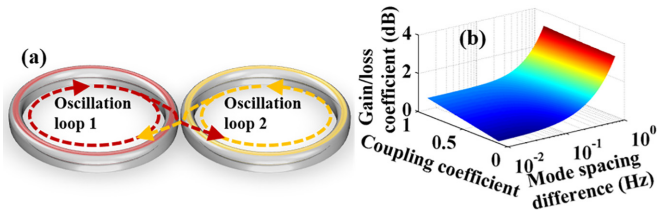

FIG. 1. (a) The energy flow between two subspaces; (b) the relationships between the gain-loss coefficient, the coupling coefficient, and the mode spacing difference.

As can be seen from Eq. (3), the single-mode oscillation occurs when the gain-loss coefficient γ_n is larger than the coupling ratio κ. Once the gain-loss coefficient γ_n is less than the coupling ratio κ, the oscillation mode will split into two frequencies. Here, the $\mathcal{PT}$-symmetry breaking condition is $\gamma_n > \kappa$.

The $\mathcal{PT}$-symmetric conditions in a dual-loop AOMO can be derived from the generic closed-loop oscillatory equations [1]. Assume that $\tilde{V}_{\text{in}}(\omega, t) = \tilde{V}_{\text{in}}e^{i\omega t}$ denotes the initial input noisy signal, and $\tilde{V}_{\text{in}}$ is the complex amplitude. Once the noise component is in the oscillator, it would circulate in the loop, and the recurrence relation of the fields is

$$\tilde{V}_n(\omega, t) = \tilde{H}_{1,2}(\omega)\lambda_{G,L}\tilde{V}_{n-1}(\omega, t - \tau_{1,2}), \tag{4}$$

where $\tilde{V}_{\text{in}}$ is the complex amplitude of the initial input noisy signal, ω is the angular frequency of the oscillation signal, and $\tilde{H}_1(\omega)$ and $\tilde{H}_2(\omega)$ are the transfer functions of the two loops forming the feedback system. The total field at any instant of time is the summation of all circulating fields. Therefore, with the input $\tilde{V}_{\text{in}}(\omega, t)$ injected into the oscillator, the signal measured at the modulation port of the modulator can be expressed as

$$\begin{aligned}\tilde{V}_{1,2}(\omega, t) &= G_A\tilde{V}_{\text{in}}\sum_{n=0}^{\infty}\tilde{H}_{1,2}(\omega)\lambda_{G,L}e^{i\omega(t-n\tau_{1,2})} \\ &= G_A\tilde{V}_{\text{in}}e^{i\omega t}/[1 - \tilde{H}_{1,2}(\omega)\lambda_{G,L}e^{-i\omega\tau_{1,2}}],\end{aligned} \tag{5}$$

where $\tilde{V}_1(\omega, t)$ and $\tilde{V}_2(\omega, t)$ are the signals in the two loops for modulation, G_A is the amplifier's amplitude gain, τ_1 and τ_2 are the delays of the two loops in the AOMO, and λ_G and λ_L are the gain and loss coefficients in each loop. As the AOMO has a similar signal flow to the structures in Refs. [20,21], according to Eq. (3) in [20] and Eq. (14) in [21], here the transfer functions are defined as

$$\tilde{H}_{1,2}(\omega) = (\Omega_B - i\omega)/[\Omega_B - i\omega - \Omega_B e^{-i\omega\tau_{1,2}}], \tag{6}$$

where Ω_B is the bandwidth of the filter in the AOMO. In a dual-loop AOMO, of which the energy flow between two subspaces is shown in Fig. 1(a), there are two oscillation parts in a dual-loop oscillator. At the coupling point of the two loops, the optical signal can be directly expressed as

$$\tilde{V}_{C-\text{all}}(\omega, t) = \tilde{V}_1(\omega, t) + \tilde{V}_2(\omega, t), \tag{7}$$

while at the point where the coupled optical signal is split into two loops and then cyclically oscillated in the two loops, the

separated optical signals are obtained as

$$\tilde{V}_{S1}(\omega,t) = \frac{G_A\tilde{V}_{\text{in}}e^{i\omega t}}{1-\tilde{H}_1(\omega)\lambda_G e^{-i\omega\tau_1}}\left[\rho+(1-\rho)\frac{1}{1-\tilde{H}_2(\omega)\lambda_L e^{-i\omega\tau_2}}\right], \tag{8}$$

$$\tilde{V}_{S2}(\omega,t) = \frac{G_A\tilde{V}_{\text{in}}e^{i\omega t}}{1-\tilde{H}_2(\omega)\lambda_L e^{-i\omega\tau_2}}\left[(1-\rho)+\rho\frac{1}{1-\tilde{H}_1(\omega)\lambda_G e^{-i\omega\tau_1}}\right]. \tag{9}$$

Under the condition $\tilde{V}_{C-\text{all}}(\omega,t)=\tilde{V}_{S1}(\omega,t)+\tilde{V}_{S2}(\omega,t)$ and assuming the coupling ratio $\rho=1/2$, there is

$$G_A\tilde{V}_{\text{in}}e^{i\omega t}\left(\frac{1}{1-\tilde{H}_1(\omega)\lambda_G e^{-i\omega\tau_1}}+\frac{1}{1-\tilde{H}_2(\omega)\lambda_L e^{-i\omega\tau_2}}\right) = 2G_A\tilde{V}_{\text{in}}e^{i\omega t}\frac{1}{1-\tilde{H}_1(\omega)\lambda_G e^{-i\omega\tau_1}}\frac{1}{1-\tilde{H}_2(\omega)\lambda_L e^{-i\omega\tau_2}}, \tag{10}$$

which can be simplified as

$$\tilde{H}_1(\omega)\lambda_G e^{-i\omega\tau_1}+\tilde{H}_2(\omega)\lambda_L e^{-i\omega\tau_2}=0. \tag{11}$$

Substituting Eq. (6) into Eq. (11), we get

$$(\Omega_B-i\omega)^2(\lambda_G e^{-i\omega\tau_1}+\lambda_L e^{-i\omega\tau_2}) - \Omega_B(\Omega_B-i\omega)e^{-i\omega(\tau_1+\tau_2)}(\lambda_G+\lambda_L)=0. \tag{12}$$

If the two loops are set to be with the same lengths, i.e., $\tau_1=\tau_2=\tau'$, Eq. (12) can be further simplified as

$$(\Omega_B-i\omega)e^{-i\omega\tau'}[(\Omega_B-i\omega)-\Omega_B e^{-i\omega\tau'}](\lambda_G+\lambda_L)=0. \tag{13}$$

Because the items of $(\Omega_B-i\omega)e^{-i\omega\tau'}$ and $(\Omega_B-i\omega)-\Omega_B e^{-i\omega\tau'}$ are not equal to zero, the following condition should be satisfied:

$$\lambda_G=-\lambda_L. \tag{14}$$

That is to say, in a dual-loop AOMO, where there is the same oscillation loop length, there must be balanced gain and loss between them. Once these two conditions are reached, according to the coupled mode theory described by Eqs. (1), (2), and (3), the coupling ratio between the two loops should be larger than the gain-loss coefficient for a stable single-mode oscillation.

III. COMPENSATION OF THE ASYMMETRIC STRUCTURE

For a $\mathcal{PT}$-symmetric oscillator with an asymmetric two-loop structure, the coupling equation can be expressed as

$$i\frac{d}{dt}\begin{pmatrix}a_n\\b_n\end{pmatrix}=\begin{pmatrix}w_m+i\gamma_{a_n} & -\kappa\\ -\kappa & w_m+w_d+i\gamma_{b_n}\end{pmatrix}\begin{pmatrix}a_n\\b_n\end{pmatrix}, \tag{15}$$

where w_d is the frequency difference of the nth mode in the two loops. If the condition of the gain and loss is satisfied, i.e., $\gamma_{a_n}=-\gamma_{b_n}=\gamma$, Eq. (15) can be written as

$$i\frac{d}{dt}\begin{pmatrix}a_n\\b_n\end{pmatrix}=\begin{pmatrix}w_m+i\gamma & -\kappa\\ -\kappa & w_m+w_d-i\gamma\end{pmatrix}\begin{pmatrix}a_n\\b_n\end{pmatrix}. \tag{16}$$

Solving the secular equation, the eigenfrequencies are given by

$$\lambda=w_m+\frac{w_d}{2}\pm\sqrt{\kappa^2+\frac{w_d^2}{4}-\gamma^2-i\gamma w_d}. \tag{17}$$

To ensure single-mode oscillation, the following condition should be satisfied:

$$\kappa^2+\frac{w_d^2}{4}-\gamma^2=0. \tag{18}$$

Thus, there exists

$$\gamma=\sqrt{\kappa^2+\frac{w_d^2}{4}}. \tag{19}$$

Figure 1(b) is plotted according to the Eq. (19). As for the coupling coefficient κ, generally, it is difficult to find the solution of the coupling coefficient. However, according to the explanation in Refs. [15,22], the coupling coefficient in the schematic diagram in Fig. 2 is determined by Slide 2. In Slide 2, the x polarization and y polarization are simply coupled without power loss. Thus, the coupling ratio is 1:1, and the coupling coefficient is 0.5, which means κ is equal to a constant. Therefore, the mode splitting induced by the asymmetric structure could be compensated by adjusting the gain-loss coefficient.

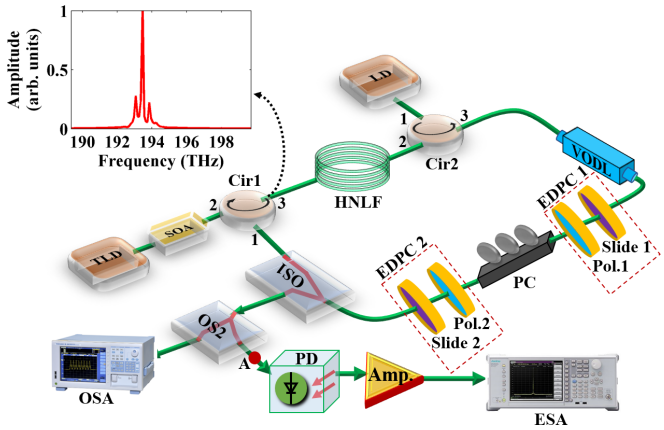

FIG. 2. Schematic diagram of the proposed $\mathcal{PT}$-symmetric AOMO.

IV. THE SINGLE-LOOP AOMO

For practical implementation of a $\mathcal{PT}$-symmetric AOMO with two physical loops, precise construction of the macro system is mandatory. Although the mode splitting induced by the asymmetric structure could be compensated by adjusting the gain-loss coefficient to a certain extent, as can be seen from Fig. 1(b), the gain-loss coefficient increases almost exponentially with the increase of mode spacing difference. For instance, if we aim for a mode spacing difference of 1 Hz employing two loops with lengths of nearly 1 m, the length

difference between them must be less than 4.9 μm, which requires an extremely sophisticated operation.

Here we propose a $\mathcal{PT}$-symmetric AOMO using a single loop, as schematized in Fig. 2. A continuous-wave light from a tunable laser diode (TLD) is launched into an SOA. At the output of the SOA, the cross-gain modulated signal is then fed into a piece of high nonlinear fiber (HNLF) through a circulator (Cir1). After transmission over the HNLF, the modulated signal copropagates with the SBS signal pumped by a laser diode (LD) through another optical circulator (Cir2) and proceeded in a variable optical delay line (VODL; Beijing Conquer Photonics Co., Ltd., KG-MODL-1000-15-S) with a delay range of 1000 ps and a minimum resolution of 4.2 fs at the operating wavelength of 1550 nm, which is used to match the loop length. The SBS signal operates as a narrow-band optical filter and an optical amplifier for the modulated signal. To develop the $\mathcal{PT}$-symmetric technique in the AOMO and realize the $\mathcal{PT}$ symmetry in the AOMO with a single ring, the all-fiber polarization elements with two cascaded electrically driven polarization controllers (EDPCs), each composed of a slide and a polarizer (Slide 1 and Pol. 1, Slide 2 and Pol. 2), are employed. The polarization of the optical signal is purified by Pol. 1 and Pol. 2. Slide 1 in front of Pol. 1 is used to change the polarization state and to increase the optical power entering Pol. 1, and Slide 2 connected behind Pol. 2 features adjusting the polarization state of the oscillation signal to keep the best modulation efficiency in the SOA. By adjusting the three-paddle polarization controller (PC) between the two polarizers, the powers of two orthogonal optical signals can be continuously controlled, which means the gain-loss coefficient can be configured. The configured optical signal is then reversely injected into the SOA to form a closed oscillation loop through the XGM-induced optical-optical modulation in the SOA.

Theoretically, the XGM is generated from photon density modulation [23]. For simplicity, the output signal of the TLD in Fig. 2 can be expressed as $A_1(0,t) = e^{j2\pi f_1 t}$. Due to the SBS-based filtering and amplification, the feedback signal in the SOA features two wavelengths. The modulation signal generated from the feedback can be written as $A_0(0,t) = e^{j2\pi f_1 t} + e^{j2\pi(f_1+f_{\rm osc})t}$, and the power of the modulation signal is $P_0(0,t) = 1$. According to the equations in Ref. [19], the optical signal at the output of the SOA can be derived as

$$A_1(L,t) = A_1(0,t)e^{(1/2)[(1-i\alpha)h-\eta_{10}A_0(0,t)A_0^*(0,t)(e^h-1)]} \times \cosh\left[\frac{1}{2}\sqrt{\eta_{02}\eta_{01}^*}A_0(0,t)A_0^*(0,t)(e^h-1)\right], \tag{20}$$

where α is the linewidth enhancement factor, h is the amplification function defined in Ref. [19], η is the coupling coefficient and $\eta_{10}(f) = \eta_{01}(-f) = \eta_{02}(f) = \eta_{20}(-f)$, and * represents conjugation. The function h can be solved according to the following simplified expression with the function approximation method:

$$\frac{dh}{dt} = -\frac{1}{(1+\varepsilon)\tau_s P_{\rm sat}}h. \tag{21}$$

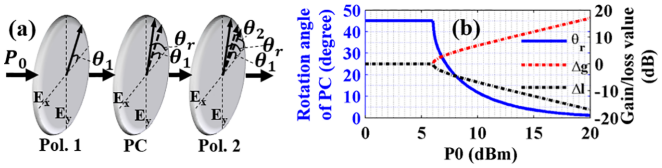

FIG. 3. (a) Illustration of the power P_0 and the polarization directions θ_1, θ_2, and θ_r; (b) the relationships among Δg, Δl, θ_r, and P_0.

Integrating by separation of variables, we get

$$h(t) = e^{-[1/(1+\varepsilon)\tau_s P_{\rm sat}]t}, \tag{22}$$

where we have used $h(0) = 1$. Substituting Eq. (22) into Eq. (20) and performing Fourier transform, we obtain the modulation spectrum of the SOA in the inset figure within Fig. 2.

Furthermore, after SBS-based amplification, the optical signals with opto-optical modulation at point A in Fig. 2 can be expressed as

$$E_A(t) = \sqrt{P_A}e^{j(2\pi f_1 t-\beta_0 L_A)}\left[\begin{matrix}\gamma_{11}e^{-j2\pi f_{\rm osc}(t-n_r L/c)}+1\\ +\Gamma\gamma_{12}e^{j2\pi f_{\rm osc}(t-n_r L/c)}e^{j\delta}\end{matrix}\right], \tag{23}$$

where P_A denotes the optical power, β_0 is the propagation constant, γ_{n1} and γ_{n2} are the modulation efficiency of the SOA, n_r is the refractive index of the TLD, L is the loop length of the oscillator, and Γ and δ are the gain coefficient and the phase shift induced by SBS, respectively.

Assuming that the power threshold of the proposed AOMO is $P_{\rm tr}$, the power at the input of Pol. 1 is P_0, the polarization directions of Pol. 1 and Pol. 2 are θ_1 and θ_2, and the rotation angle of the polarization direction introduced by the PC is θ_r, as shown in Fig. 3(a). Firstly, if the polarization directions of Pol. 1 and Pol. 2 in Fig. 3(a) are not aligned, the power of the injected optical signal from Pol. 1 with polarization direction θ_1 will be attenuated by $\cos^2(\theta_2-\theta_1)$, thus the optical power satisfies $P_1 = P_0\kappa\cos^2(\theta_2-\theta_1)$. Then, the polarization direction of the injected optical signal from Pol. 1 is adjusted to θ_r. Obviously, the powers of the two orthogonal optical signals at the output of Pol. 2 can be respectively expressed as

$$P_{{\rm out}-x} = P_1\cos^2(\theta_r) = P_0\kappa\cos^2(\theta_2-\theta_1)\cos^2(\theta_r), \tag{24}$$

$$P_{{\rm out}-y} = P_1\sin^2(\theta_r) = P_0\kappa\cos^2(\theta_2-\theta_1)\sin^2(\theta_r). \tag{25}$$

As an example, assume that the signal in x polarization exhibits a gain coefficient Δg, while the y-polarization direction has a loss coefficient Δl, and Pol. 2 is aligned with Pol. 1. According to Ref. [11], there are $\Delta g = P_{{\rm out}-x} - P_{\rm tr}$, $\Delta l = -(P_{\rm tr} - P_{{\rm out}-y})$. Under the measurement unit decibel milliwatts, the gain-loss coefficients can be expressed as

$$\begin{aligned}\Delta g &= 10lg[P_0\kappa\cos^2(\theta_r)] - 10lg(P_{\rm tr})\\ &= 10lg[P_0\kappa\cos^2(\theta_r)/P_{\rm tr}],\end{aligned} \tag{26}$$

$$\begin{aligned}\Delta l &= 10lg[P_0\kappa\sin^2(\theta_r)] - 10lg(P_{\rm tr})\\ &= 10lg[P_0\kappa\sin^2(\theta_r)/P_{\rm tr}].\end{aligned} \tag{27}$$

According to the $\mathcal{PT}$-symmetric condition $\Delta g = -\Delta l$, the relationship between θ_r and P_0 can be written as

$$\theta_r = \tfrac{1}{2}\arcsin[2P_{\rm tr}/(P_0\kappa)]. \tag{28}$$

In the single-loop AOMO, the coupling ratio κ and the power threshold $P_{\rm tr}$ are set to be 0.5 and 0 dBm. According to Eq. (28), the minimum of P_0 can be derived as $P_{0\_\min} = 10lg(2P_{\rm tr}/\kappa)$. The relationships among Δg, Δl, θ_r, and P_0 are plotted in Fig. 3(b). As seen from Fig. 3(b), when the power at the input of Pol. 1 is higher than a certain value, the gain-loss condition can be reached by adjusting the polarization direction at the PC.

V. PHASE NOISE ANALYSIS

The Yao-Maleki model [1] and the Leeson model [24] have provided the basic approaches to phase noise analysis of feedback oscillators and focused on the white noise, such as the relative intensity noise (RIN) of the laser, shot noise of the photodiode, thermal noise of the active electronic devices, and $1/f$ noise. Here in the AOMO, the phase noise is mainly affected by the RIN noise of the laser, the SBS-induced additive noise, the SBS-induced amplified spontaneous emission (ASE) noise, and the optical amplifier (including the SOA) -induced ASE noise. By analyzing the evolution of the signal phase [20,25–28], the phase noise of the detected electrical signal can be formulated as

$$\mathcal{L}_{\rm OEO}(f) = \begin{bmatrix} S_{\rm noise-floor}(f) + S_{\rm SBS}(f) \\ +S_{\rm ASE-SBS}(f) + S_{\rm ASE-OA}(f) \end{bmatrix} |H_{\rm OEO}(jf)|^2/2, \tag{29}$$

where

$$S_{\rm noise-floor}(f) = \frac{N_{\rm RIN} I_{ph}^2 Z_0}{P_{\rm rf}}, \tag{30}$$

$$S_{\rm SBS}(f) = \left[\frac{\eta_{12} e^{g_p I_p L}}{\eta_{11} + \eta_{12} e^{g_p I_p L}} \frac{g_p I_p L}{\Delta\nu_B}\right]^2 [S_{\nu\_s1}(f) + S_{\nu\_p0}(f)], \tag{31}$$

$$S_{\rm ASE-SBS}(f) = \frac{R_{PD}^2 Z_0 P_c}{2\eta P_{\rm rf,}} h\nu_s n_{\rm sp} \left\{ e^{kl(f)(1-e^{-\rho L})} \begin{bmatrix} 1/[kl(f)] \\ +e^{-\rho L} \end{bmatrix} \right\}, \\ -1 - 1/[kl(f)] \tag{32}$$

$$S_{\rm ASE-OA}(f) = \frac{2R_{PD}^2}{\eta} P_c (G-1) n_{\rm sp} h f_\upsilon, \tag{33}$$

$$H_{\rm OOMO}(jf) = \frac{\Delta\nu_B - j2\pi f}{\Delta\nu_B - j2\pi f - \Delta\nu_B e^{-j2\pi f\tau}}. \tag{34}$$

$S_{\rm noise-floor}(f)$ is the noise floor, $S_{\rm SBS}(f)$ is the SBS-induced additive phase noise spectrum, $S_{\rm ASE-SBS}(f)$ is the SBS-induced ASE noise spectrum, $S_{\rm ASE-OA}(f)$ is the ASE noise spectrum induced by optical amplifiers (including SOAs), $H_{\rm OOMO}(jf)$ is the transfer function of the oscillation system, q is the charge of an electron, Z_0 is the load resistance of the photodiode (PD), $I_{\rm ph}$ is the photocurrent at the output of the PD, $N_{\rm RIN}$ is RIN of the TLD, $P_{\rm rf}$ is the rf power at the output of PD, g_p is the line center Brillouin gain coefficient, $I_p = P_p/A_{\rm eff}$ is the power intensity of the LD, P_p is the power of the LD, $A_{\rm eff}$ is the effective mode area, L is the length of the HNLF, $\Delta\nu_B$ is the gain bandwidth of SBS, $S_{\nu\_s1}(f) = B_{s1}(1+\gamma_{s1}|f|)/(2\pi f^2)$ and $S_{\nu\_p0}(f) = B_{p0}(1+\gamma_{p0}|f|)/(2\pi f^2)$ are the power spectral density of optical frequency noise for the TLD and LD, B_{s1} and B_{p0} are the linewidths of the two lasers, γ_{s1} and γ_{p0} are the $1/f$ break frequency, $R_{\rm PD}$ is the responsivity of the PD, η is the quantum efficiency of the PD, h is the Planck's constant, ν_s is the optical frequency of the Stokes wave, $n_{\rm sp} = 1 + (e^{h\nu_B/(\kappa T)} - 1)^{-1}$ is the spontaneous emission factor, ν_B is the frequency shift of SBS, κ is the Boltzmann's constant, T is the room temperature, $k = g_p P_p/(\rho A_{\rm eff})$, ρ is the power loss of HNLF, $l(f) = (\Delta\nu_B/2)^2/[f^2 + (\Delta\nu_B/2)^2]$, f is the offset frequency, P_c is the power of optical carrier, τ is the time delay of HNLF, G is the amplifier gain, f is the offset frequency, and f_υ is the optical frequency.

The phase noise performance of the proposed OOMO is simulated based on the above models, which is shown in Fig. 4(e). The following parameters are used in the simulation: $\eta_{n1} = -\eta_{n2} = -0.1$, $Z_0 = 50\ \Omega$, $A_{\rm eff} = 63.6 \times 10^{-12}$ m^2, $g_p = 2 \times 10^{-11}$m/W, $\Delta\nu_B = 20$ MHz, the wavelengths of the TLD are 1550 nm, $P_p = 20$ dBm, $P_c = 0$ dBm, $\nu_B = 10.7$ GHz, $I_{\rm ph} = 4 \times 10^{-3}$ A, $R_{\rm PD} = 0.56$, $B_{s1} = B_{p0} = 100$ Hz, $\gamma_{s1} = \gamma_{p0} = 20$ Hz, $T = 300$ K, $N_{\rm RIN-}{}_m = -150$ dB/Hz, $\kappa = 1.380\,649 \times 10^{-23}$, $h = 6.626\,070\,15 \times 10^{-34}$, $q = 1.602\,189\,2 \times 10^{-19}$, $\eta = 0.45$, and $\rho = -1.5$ dB. As can be seen from Fig. 4(e), the theoretical phase noise performance of the system at 10 kHz offset frequency is limited to about -118.4 dBc/Hz, which can be greatly improved by using the LD with narrower linewidth and lower power and the HNLF with longer length.

VI. EXPERIMENTAL RESULTS

We experimentally verified the proposed $\mathcal{PT}$-symmetric AOMO with a single loop based on the configuration shown in Fig. 2. A lightwave with an optical power of 2.5 dBm from the TLD (NKT Photonics, Koheras AdjustiK E15) is injected into the SOA (Aeon SAC20r) biased at 400 mA. After the Cir1, a 200 m HNLF (YOFC, NL1550-zero) with zero dispersion coefficient is used as the SBS gain medium and the delay unit, in which the SBS pump power from the LD (NKT Photonics, Koheras AdjustiK E15) is 16 dBm. The LD operates at a fixed wavelength to enhance the system's stability. After transmission over the two cascaded EDPCs (Phoenix Photonics, PWP-02-15-PM-2-1), the optical signal is split by a 30:70 optical splitter (OS1), 30% of which is injected into a 50:50 optical splitter (OS2). At the output of the OS2, one part of the signal is used to illuminate a PD (Finisar, XPDV2120RA) for spectrum and phase noise measurements using an electrical spectrum analyzer (ESA; Anritsu MS2840A), and the other is injected into an optical spectrum analyzer for wavelength monitoring (Finisar 1500s).

The optical spectrum of the oscillatory dual-wavelength signal with 10 GHz spacing is shown in Fig. 4(a). The suppression ratio of the unwanted modulation sideband is more than 17 dB. The electrical spectra at the PD output are shown in Fig. 4(b) when the frequency is tunable in the range of 3–30 GHz by adjusting the wavelength of the TLD. The side-mode suppression ratios (SMSRs) are displayed in Figs. 4(c) and 4(d), reaching 44.96 and 39.671 dB at frequencies of 10

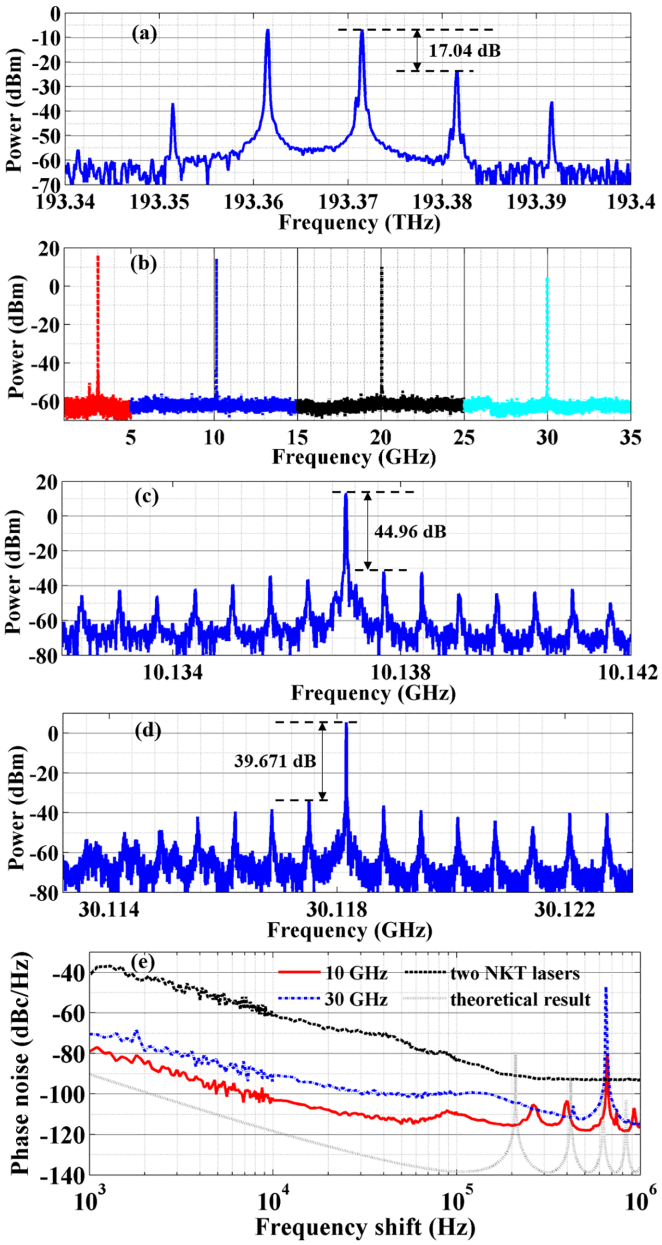

FIG. 4. Spectra analysis. (a) The optical spectra of the oscillatory dual-wavelength signal; (b) the electrical spectra of the beating signal with wideband tunability; (c) the electrical spectrum at 10 GHz; (d) the electrical spectrum at 30nbsp;GHz; (e) the phase noise results.

and 30 GHz. We also measured the phase noise performance of the oscillation signal by beating the TLD and LD. As shown in Fig. 4(e), the phase noise at the frequency spacings of 10 and 30 GHz are as low as −103.2 and −90.69 dBc/Hz at 10 kHz frequency offset, which is 42.52 and 30.01 dB less than the phase noise between the two NKT lasers with an ultranarrow linewidth of 100 Hz, and this can be further improved with a longer loop length. It is noted that the phase noise result at 10 GHz outperforms the AOMOs previously reported with dual-loop configurations, which are in the range of −81.27 to −95 dBc/Hz. Here the phase noise and SMSR of 10 GHz spacing are better than at 30 GHz spacing because the modulation efficiency at the SOA decreases with the increase

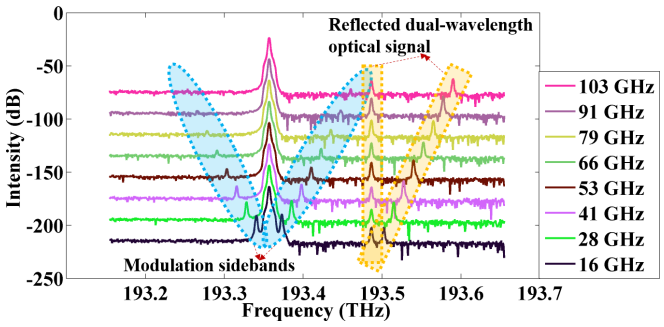

FIG. 5. Optical spectra of the modulation intensity vs the frequency gap.

of modulation frequency. In addition, due to the imperfect performances of the devices and the existence of noise floor in the ESA in the experiment, the measured phase noise is worse than the theoretically calculated value.

In the experiment, the XGM modulation frequency is determined by the frequency gap between the optical carrier from the TLD and the LD-induced SBS signal. The LD operates at a fixed wavelength to enhance the system's stability, and the XGM modulation frequency is tuned by adjusting the wavelength of the TLD. We measured the modulation capability of the SOA by inversely injecting a dual-wavelength optical signal into the SOA, which is shown in Fig. 5. As can be seen, the modulation intensity decreases with the frequency gap increase. When the frequency gap reaches 41 GHz, the powers of the modulation sidebands are still much higher than the noise. During the experiment, we measured the single-mode oscillation frequency up to 40 GHz. However, the stably oscillated frequency was limited to about 30 GHz.

Moreover, to exploit the stability of the proposed $\mathcal{PT}$-symmetric AOMO, the frequency drifts and the power fluctuations at frequencies of 10 and 30 GHz are evaluated, as shown in Figs. 6(a) and 6(b). The whole system is placed in a constant temperature environment and on an optical table to reduce the impact of environmental factors. The ESA operates in "max hold" mode for more than 100 s with a frequency span of 1 MHz. No mode hopping is observed, and the oscillation frequency drift is about 100 kHz with a power fluctuation of about 2 dB, which could be compensated by electrically controlling the effective length of the VODL.

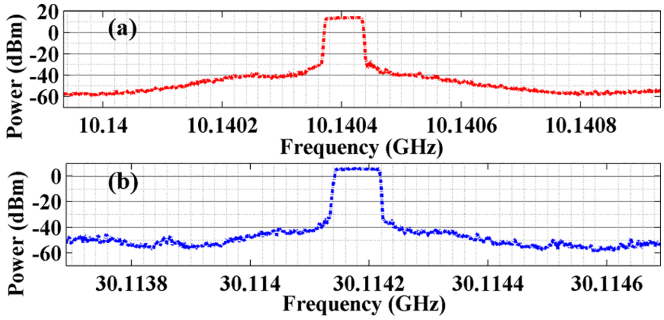

FIG. 6. The stability performances of the system for 100 s at oscillation frequencies of (a) 10 GHz and (b) 30 GHz.

VII. CONCLUSION

In conclusion, we propose and experimentally demonstrate a simple single-loop $\mathcal{PT}$-symmetric AOMO. The $\mathcal{PT}$ symmetry is realized by constructing a polarimetric signal flow in the oscillation loop. By controlling the polarization state of the PC in the $\mathcal{PT}$-symmetric structure, two mutually coupled loops with balanced gain and loss can be easily conceived. Using the XGM in the SOA, the SBS-based frequency selection, and the $\mathcal{PT}$-symmetric breaking, dual-wavelength optical signals in a wideband with low beating phase noise are tunable and stably generated from our proposed AOMO. The measured phase noise of 10 GHz in the experiment reaches less than −103.2 dBc/Hz at a 10 kHz frequency offset, much better than that of beating two free-running cutting-edge lasers. The proposed scheme realizes an ultranarrow microwave photonic oscillator and is expected to have a high potential in applications in the microwave photonics community.

ACKNOWLEDGMENT

This work was supported by the National Natural Science Foundation of China (Grant No. 62101508).

[1] X. S. Yao and L. Maleki, Optoelectronic microwave oscillator, JOSA B **13**, 8 (1996).

[2] J. Yang, Y. Jin-Long, W. Yao-Tian, Z. Li-Tai, and Y. En-Ze, An optical domain combined dual-loop optoelectronic oscillator, IEEE. Photonics Technol. Lett. **19**, 11 (2007).

[3] Z. Tamir, A. Meltzer, and M. Horowitz, Wideband tunable optoelectronic oscillator based on frequency translation, Opt. Lett. **42**, 14 (2017).

[4] Y. Jiang, G. Bai, L. Hu, H. Li, Z. Zhou, J. Xu, and S. Wang, Frequency locked single-mode optoelectronic oscillator by using low frequency RF signal injection, IEEE. Photonics Technol. Lett. **25**, 4 (2013).

[5] A. Banerjee, L. Aguiar Dantas de Britto, and G. M. Pacheco, Analysis of injection locking and pulling in single-loop optoelectronic oscillator, IEEE Trans. Microwave Theory Tech. **67**, 5 (2019).

[6] C. E. Rüter, K. G. Makris, R. El-Ganainy, D. N. Christodoulides, M. Segev, and D. Kip, Observation of parity–time symmetry in optics, Nat. Phys. **6**, 192 (2010).

[7] B. Peng, Ş. Kaya Özdemir, F. Lei, F. Monifi, M. Gianfreda, G. L. Long, S. Fan, F. Nori, C. M. Bender, and L. Yang, Parity–time-symmetric whispering-gallery microcavities, Nat. Phys. **10**, 394 (2014).

[8] H. Hodaei, M.-A. Miri, M. Heinrich, D. N. Christodoulides, and M. Khajavikhan, Parity-time–symmetric microring lasers, Science **346**, 6212 (2014).

[9] L. Feng, Z. J. Wong, R.-M. Ma, Y. Wang, and X. Zhang, Single-mode laser by parity-time symmetry breaking, Science **346**, 6212 (2014).

[10] J. Zhang and J. Yao, Parity-time–symmetric optoelectronic oscillator, Sci. Adv. **4**, 6 (2018).

[11] Y. Liu, T. Hao, W. Li, J. Capmany, N. Zhu, and M. Li, Observation of parity-time symmetry in microwave photonics, Light: Sci. Appl. **7**, 38 (2018).

[12] Z. Fan, W. Zhang, Q. Qiu, and J. Yao, Hybrid frequency-tunable parity-time symmetric optoelectronic oscillator, J. Lightwave Technol. **38**, 8 (2020).

[13] H. Tang, Y. Yu, and X. Zhang, Widely tunable optoelectronic oscillator based on selective parity-time-symmetry breaking, Optica **6**, 8 (2019).

[14] J. Zhang, L. Li, G. Wang, X. Feng, B.-O. Guan, and J. Yao, Parity-time symmetry in wavelength space within a single spatial resonator, Nat. Commun. **11**, 3217 (2020).

[15] P. Li, Z. Dai, Z. Fan, L. Yan, and J. Yao, Parity–time-symmetric frequency-tunable optoelectronic oscillator with a single dual-polarization optical loop, Opt. Lett. **45**, 3139 (2020).

[16] S. Wang, Z. Lu, W. Li, S. Jia, L. Zhang, M. Qiao, X. Pang, N. Idrees, M. Saqlain, X. Gao, X. Cao, C. Lin, and Q. Wu, Xianmin Zhang, and Xianbin Yu, 26.8-m THz wireless transmission of probabilistic shaping 16-QAM-OFDM signals, APL Photonics **5**, 056105 (2020).

[17] Y. Jiang, Y. Zi, G. Bai, and J. Tian, All-optical microwave oscillator based on semiconductor optical amplifier and stimulated Brillouin scattering, Opt. Lett. **43**, 8 (2018).

[18] J. Tang, G. Bai, Y. Tang, L. Xu, G. Wang, D. Shang, and Y. Jiang, All-optical microwave oscillator based on a mutual-injection coupling between DFB-LDs, Opt. Express **30**, 23 (2022).

[19] S. Junqiang, Z. Xinliang, L. Deming, and H. Dexiu, Analytical solution of four-wave mixing between picosecond optical pulses in semiconductor optical amplifiers with cross-gain modulation and probe depletion, Microwave Opt. Technol. Lett. **28**, 78 (2001).

[20] H. Peng, C. Zhang, X. Xie, T. Sun, P. Guo, X. Zhu, L. Zhu, W. Hu, and Z. Chen, Tunable DC-60 GHz RF generation utilizing a dual-loop optoelectronic oscillator based on stimulated Brillouin scattering, J. Lightwave Technol. **33**, 2707 (2015).

[21] Y. Wang, S. Qiu, M. Yang, S. Shen, and S. Li, Wideband frequency-tunable optoelectronic oscillator with ultranarrow linewidth based on stimulated Brillouin scattering, Opt. Commun. **546**, 129734 (2023).

[22] Z. Fan, Z. Dai, Q. Qiu, and J. Yao, Parity-time symmetry in a single-loop photonic system, J. Lightwave Technol. **38**, 3866 (2020).

[23] T. Durhuus, B. Mikkelsen, C. Joergensen, S. L. Danielsen, and K. E. Stubkjaer, All-optical wavelength conversion by semiconductor optical amplifiers, J. Lightwave Technol. **14**, 6 (1996).

[24] D. B. Leeson, A simple model of feedback oscillator noise spectrum, Proc. IEEE **54**, 329 (1966).

[25] M. J. O'Mahony and I. D. Henning, Semiconductor laser linewidth broadening due to $1/f$ carrier noise, Electron. Lett. **19**, 1000 (1983).

[26] G. Duan and E. Georgiev, Non-white photodetection noise at the output of an optical amplifier: Theory and experiment, IEEE J. Quantum Electron. **37**, 8 (2001).

[27] H. Peng, Y. Xu, X. Peng, X. Zhu, R. Guo, F. Chen, H. Du, Y. Chen, C. Zhang, L. Zhu, W. Hu, and Z. Chen, Wideband tunable optoelectronic oscillator based on the deamplification of stimulated Brillouin scattering, Opt. Express **25**, 9 (2017).

[28] F. Francis and R. Manivasakan, On the theoretical performance limits of long repeated/regenerated optical IMDD links, version 1 (2021), doi:https://doi.org/10.21203/rs.3.rs-615471/v1.